



A 14 year dataset of in situ glacier surface velocities for a tidewater and a land-terminating glacier in Livingston Island, Antarctica

Francisco Machío¹, Ricardo Rodríguez-Cielos², Francisco Navarro³, Javier Lapazaran³, Jaime Otero³

5

(1) Escuela Superior de Ingeniería y Tecnología, Universidad Internacional de La Rioja (UNIR), Calle Almansa, 101, 28040 Madrid, Spain.

(2) Departamento de Señales, Sistemas y Radiocomunicaciones, ETSI de Telecomunicación, Universidad Politécnica de Madrid, Av. Complutense, 30, 20040 Madrid, Spain.

10 (3) Departamento de Matemática Aplicada a las Tecnologías de la Información y las Comunicaciones, ETSI de Telecomunicación, Universidad Politécnica de Madrid, Av. Complutense, 30, 20040 Madrid, Spain.

Correspondence to: Francisco Machío (francisco.machio@unir.net)

Abstract

15 We present a 14 year record of in situ glacier surface velocities determined by repeated GNSS measurements at a dense net of 52 stakes distributed across two glaciers, Johnsons (tidewater) and Hurd (land-terminating), located on Livingston Island, South Shetland Islands, Antarctica. The measurements cover the period 2000-2013 and were done at the beginning and end of each austral summer season. A second-degree polynomial approximation is calculated for each stake, which allows estimating the approximate velocities at intermediate times. This dataset can be useful as input data to numerical models of glacier dynamics, or for calibration and validation of remotely sensed velocities such as D-
20 inSAR or SAR offset/coherence tracking velocities, for a region where very scarce in situ glacier surface velocity measurements are available.

Link to the data repository: <http://doi.pangaea.de/10.1594/PANGAEA.846791>.

1. Introduction

25 In situ measured glacier-surface velocities are an important source of information for glacier dynamics studies. The strain field is defined in terms of velocity gradients, and the stresses in terms of strains through the constitutive relationship (most often Nye's generalization of Glen's law; e.g. Cuffey and Paterson, 2010, ch. 3). The velocity field gradients are thus responsible for observed deformation patterns such as e.g. folding or foliation, and damage expressions such as fracturing, faulting and crevassing (Hambrey and Lawson, 2000; Ximenis et al., 2000). Furthermore, observed surface velocities can give an insight on basal conditions. In particular, they have been used since long ago to
30 infer basal drag (e.g. van der Veen and Whillans, 1989; Hooke et al., 1989).

Observed surface velocities are commonly used as input data to numerical models. Here, they could be directly used as Dirichlet boundary conditions at the glacier surface for the velocity field. However, most often traction-free boundary conditions (i.e. Neumann conditions) are set at the glacier surface, and the velocities are used instead for tuning model's free parameters such as the viscosity coefficient in the constitutive relationship or the basal drag coefficient in the sliding
35 law. For long time, the numerical simulations considered such coefficients as constant over the entire glacier (e.g. Hanson, 1995; Martín et al., 2005; Otero et al., 2010). Recently, it is becoming more and more usual to establish the viscosity and/or the basal drag coefficients as functions of position. This is done by means of inversion procedures that heavily rely on observed velocities at the glacier surface. For instance, in the method introduced by Arthern and Gudmundsson (2010) and modified by Jay-Allemand et al. (2011), the surface velocities are used to solve the Dirichlet problem involved in the inverse Robin problem solving for the viscosity or basal drag coefficients. However, these inversion procedures require a large amount of measured velocities, which is seldom available from in situ measurements and thus recommend the use of remotely-sensed velocities, such as Interferometric SAR, SAR offset tracking or SAR coherence tracking velocities (e.g. Strozzi et al., 2002; Rignot and Kanagaratnam, 2006; Joughin et al.,
40 2010; Wuite et al., 2015). But even in these cases in situ-measured glacier velocities are still of much interest, since they provide a means for calibration and validation of remotely-sensed velocities (e.g. Strozzi et al., 2008; Schellenberger et al., 2015). This is of interest in view of the recent efforts to derive time series for regional or global ice-velocity fields such as those involved in the MEaSUREs program (<https://nsidc.org/data/nsidc-0484/versions/2>, accessed on 07/05/2017), GoLIVE project (<https://nsidc.org/data/golive>, accessed on 07/05/2017) and ENVEO CryoPortal (<http://cryoportale.enveo.at/>, accessed on 07/05/2017).



In this paper, we present a 14 year record of in situ glacier surface velocities determined by repeated GNSS measurements at a dense net of stakes on two glaciers, Johnsons and Hurd, located on Livingston Island, South Shetland Islands (Fig. 1). These islands, located off the north-western tip of the Antarctic Peninsula, previously had a scarce record of in situ velocity observations, which included measurements in the late 1980s in Nelson Island (Ren Jiaven et al., 1995), earlier measurements in the late 1990s in Johnsons Glacier (Ximenis et al., 1999), and measurements in the Arctowski Icefield, the Bellingshausen Dome and the Central Dome of King George Island between 1999/2000 and 2008/09 (Blindow et al., 2010; Rückamp et al., 2010, 2011). Such in situ velocity measurements are critical for validation of the estimates of remote-sensor-based studies of ice discharge in the region such as those by Osmanoglu et al. (2013, 2014) for King George and Livingston islands, respectively. An added interest of the presented velocity record is that it corresponds to both a tidewater glacier and a land-terminating glacier, two typical, but very different in dynamical behaviour, glacier types in this region.

2. Geographical setting

Our study area is Hurd Peninsula ($62^{\circ} 39\text{--}42' \text{ S}$, $60^{\circ} 19\text{--}25' \text{ W}$), located in the south of Livingston Island, South Shetland Archipelago, Antarctica. This peninsula is the setting of Juan Carlos I Station (JCI), which provided the logistic support for our fieldwork (Fig. 1). Hurd Peninsula is covered by an ice cap that extends over an area of about 13.5 km^2 and spans an altitude range from sea level to about 370 m.a.s.l. It is partly surrounded by mountains that reach between 250 and 400 meters in height.

This ice cap can be divided into two main glacier systems. The first main unit is Johnsons Glacier, a tidewater glacier, mostly flowing north-westwards, which ends on a calving front of about 50 m in height, of which just a few meters (typically $< 10 \text{ m}$) are submerged. This calving front extends approximately 500–600 m along the coast. The second main unit is Hurd glacier, flowing mostly south-westwards and terminating on land, with three main lobes named Sally Rocks (flowing south-westwards), Las Palmas (flowing westwards) and Argentina (flowing north-westwards). There are three additional smaller basins, all flowing eastwards to False Bay, which were excluded from this study because they are heavily crevassed icefalls which prevent safe field measurements.

The local ice divide separating Johnsons and Hurd lies between 250 and 330 m.a.s.l. (Fig. 1). Hurd Glacier has an average surface slope of about 3° , though the small westward flowing glacier tongues Argentina and Las Palmas are steeper, around 13° . Typical surface slopes for Johnsons Glacier range between 10° in its northern areas and 6° in the southern ones.

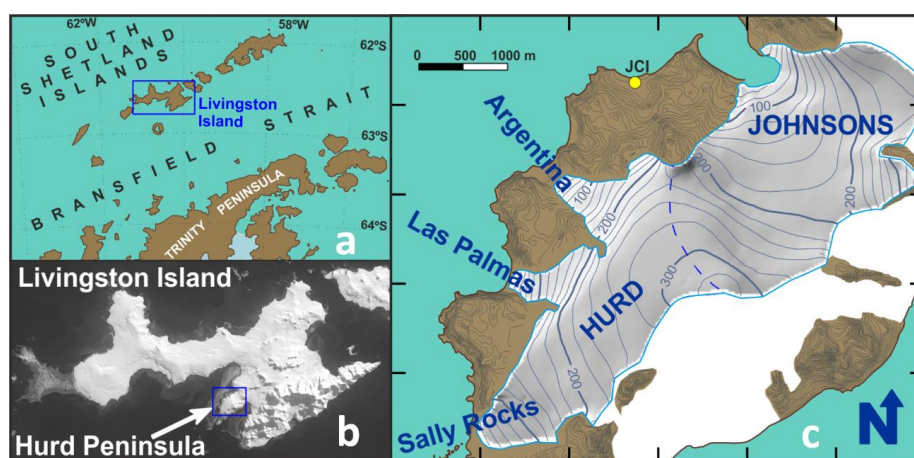


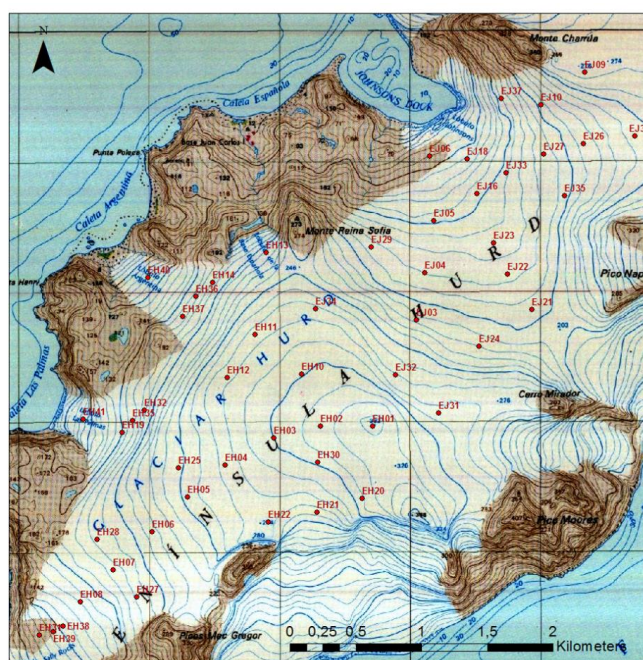
Fig. 1. a) Location of Livingston Island in the South Shetland Archipelago. b) Situation of Hurd Peninsula on Livingston Island (orthophoto generated from SPOT 1991 image by Universitat de Barcelona and Institut Cartogràfic de Catalunya, 1992). c) Location and surface elevation map of Hurd and Johnsons Glaciers, Hurd Peninsula, Livingston Island. The dashed blue line indicates the ice divide separating Hurd and Johnsons Glaciers. Elevations and outline are based on a survey during summer 1998/99 and 2000/01. A yellow dot shows the position of Juan Carlos I Station (JCI).



The Hurd Peninsula ice cap is a polythermal ice mass, showing an upper layer of cold ice, several tens of meters thick, in the ablation zone. This layer is rather uniformly distributed in Hurd Glacier, while it has a patchy distribution in Johnsons Glacier (Navarro et al., 2009). In the snouts of Hurd Glacier (in Sally Rocks area) and its side lobes Argentina and Las Palmas, where the glacier thickness tapers to zero, the cold ice layer extends down to bedrock, so the glacier is frozen to the bed, implying a compressional stress regime. In contrast, the area close to Johnsons calving front shows the extensional stress regime characteristic of the terminus of tidewater glaciers (Molina et al., 2007; Navarro et al., 2009; Otero et al., 2010).

The average ice thickness of the joint Hurd-Johnsons, determined from ground-penetrating radar data in 2000/2001, was 93.6 ± 2.5 m, with maximum values about 200 m, in the accumulation area of Hurd Glacier, and only about 160 m in Johnsons Glacier (Navarro et al., 2009). Johnsons Glacier bed is rather regular, with altitudes decreasing towards the ice front, where glacier bed elevation is slightly below sea level (typically < 10 m). Hurd Glacier bed, however, is more irregular, with a clear over-deepening in the thickest ice area, close to the head of Argentina side lobe, and another one, though less pronounced, near the head of Las Palmas side lobe.

The Hurd Peninsula ice cap is subjected to the maritime climate of the western Antarctic Peninsula (AP) region. The annual average temperature at JCI during the period 1994-2014 was -1.2°C , with average summer (DJF) and winter (JJA) temperatures of 1.9°C and -4.7°C , respectively (Bañón and Vasallo, 2016). The surface mass balance over the period 2002-2011 has been close to zero for both glaciers: 0.05 ± 0.30 mm w.e. for Johnsons and -0.15 ± 0.44 mm w.e. for Hurd (the range indicates the standard deviation). The latter has shown a slightly more negative balance because of its lower accumulation rates, attributed to snow redistribution by wind, together with slightly higher ablation rates, due to Hurd's hypsometry, which shows a much larger share of area at the lowermost altitudes (< 100 m) as compared with Johnsons (Navarro et al., 2013). The average accumulation area ratios over the same period were 44 ± 24 % for Hurd Glacier and 61 ± 21 % for Johnsons Glacier (again, quoted the standard deviations). Their equilibrium line altitudes (ELA) for the same period were 228 ± 57 m a.s.l. and 187 ± 37 m a.s.l., respectively (Navarro et al., 2013).



25

Fig. 2. Net of stakes on Hurd and Johnsons Glaciers at the end of the 2012-2013 Antarctic summer campaign. (Base map: SGE, 1990).



3. Methods

The glacier surface velocities were measured by precise repeated positioning measurements by GNSS techniques on a net of stakes deployed by the authors on Johnsons and Hurd glaciers (Fig. 2). The net of stakes consisted (as of the end of the measurement period reported) of 22 stakes for Johnsons and 30 stakes for Hurd Glacier. The stakes were surveyed 2-4 times per summer campaign during the period 2000-2013. The GNSS measurements were done using a Trimble 5700 system, with Data Controller TSC2. The measurements were done either in real-time kinematics (RTK) or in fast-static (post-processed) mode; for the latter, an occupation time of 10 s was set. In general, RTK mode was used, but in some cases a radio link to the base station was not available, and fast-static mode was employed. The GNSS base station was located at the neighbouring Juan Carlos I Station (Fig. 1). This is a permanent GNSS station with coordinates determined with an accuracy better than 5 cm in horizontal and 2 cm in vertical. The estimated horizontal accuracy for the stake positions lies between 0.07 and 0.60 m. The main contributor to this uncertainty is not the GNSS measurement error (average values of 7 and 10 cm for horizontal and vertical positioning, respectively) but the estimated uncertainties in the correction for tilt of the stakes.

From the collected observations of stake positioning, a surface velocity map can be obtained by applying the procedure described below. We will just focus on horizontal velocities, since the vertical component of the velocity is very small, and prone to errors such as those of tilt of the stake. From the known position (x_{t_n}, y_{t_n}) of a stake at a given time t_n (expressed in days since the zero time for observations, t_0 , which we arbitrarily set as 01/01/1999 at 00:00), with the subscript n indicating the sequential number of the observation, we define:

$$\begin{aligned}\Delta x_{t_{n-1}}^{t_n} &= x_{t_n} - x_{t_{n-1}} \\ \Delta y_{t_{n-1}}^{t_n} &= y_{t_n} - y_{t_{n-1}} \\ \Delta X &= \sum_{i=2}^n \Delta x_{t_{i-1}}^{t_i} \\ \Delta Y &= \sum_{i=2}^n \Delta y_{t_{i-1}}^{t_i}\end{aligned}\quad (1)$$

In this way, the planimetric position of a stake over time is defined by the discrete functions

$$\begin{aligned}X(t_n) &= X(x_{t_1}, x_{t_1} + \Delta x_{t_1}^{t_2}, \dots, x_{t_1} + \Delta X) \\ Y(t_n) &= Y(y_{t_1}, y_{t_1} + \Delta y_{t_1}^{t_2}, \dots, y_{t_1} + \Delta Y)\end{aligned}\quad (2)$$

It is possible to adjust the previous functions by means of second-order polynomials, which is equivalent to assuming that the stake moves with constant acceleration:

$$\begin{aligned}X_a(t_n) &= a_x t_n^2 + b_x t_n + c_x \\ Y_a(t_n) &= a_y t_n^2 + b_y t_n + c_y\end{aligned}\quad (3)$$

This set of two equations, with three unknowns each, will have a solution, or a better approximation to it, if sufficient observations ($n \geq 3$) are available for each stake.

The unknown coefficients are determined by least-square fitting, minimizing the residual vectors

$$\begin{aligned}\mathbf{R}_x &= \begin{bmatrix} t_1^2 & t_1 & 1 \\ t_2^2 & t_2 & 1 \\ \dots & \dots & \dots \\ t_n^2 & t_n & 1 \end{bmatrix} \begin{bmatrix} a_x \\ b_x \\ c_x \end{bmatrix} - \begin{bmatrix} X(t_1) \\ X(t_2) \\ \dots \\ X(t_n) \end{bmatrix} = \mathbf{A}\mathbf{C}_x - \mathbf{X} \\ \mathbf{R}_y &= \begin{bmatrix} t_1^2 & t_1 & 1 \\ t_2^2 & t_2 & 1 \\ \dots & \dots & \dots \\ t_n^2 & t_n & 1 \end{bmatrix} \begin{bmatrix} a_y \\ b_y \\ c_y \end{bmatrix} - \begin{bmatrix} Y(t_1) \\ Y(t_2) \\ \dots \\ Y(t_n) \end{bmatrix} = \mathbf{A}\mathbf{C}_y - \mathbf{Y}\end{aligned}\quad (4)$$

By minimizing the above residuals for each of the existing stakes, we will get the adjusted functions, $X_a(t_n)$ and $Y_a(t_n)$, which allow to estimate how the position of each stake evolves with time.

The horizontal velocity of a stake will be given, from the time derivatives of the positions, by the expressions:

$$\begin{aligned}\mathbf{v} &= v_x \mathbf{i} + v_y \mathbf{j} \\ v_x &= X_a'(t_n) = 2 a_x t_n + b_x \\ v_y &= Y_a'(t_n) = 2 a_y t_n + b_y \\ v_{xy} &= \sqrt{v_x^2 + v_y^2}\end{aligned}\quad (5)$$



To obtain the error estimates e_x and e_y (from which we calculate $e_{xy} = \sqrt{e_x^2 + e_y^2}$) of the adjusted functions, $X_a(t_n)$ and $Y_a(t_n)$, we follow the parametric adjustment procedure (see details in Ghilani, 2010), which has to be applied separately for X and Y (for brevity, we just describe it below for X). For a least-square fit, these equations are:

$\mathbf{N} = [\mathbf{A}^T \mathbf{A}]$ $\mathbf{C}_x = \mathbf{N}^{-1} [\mathbf{A}^T \mathbf{X}]$ $\mathbf{R}_x = \mathbf{A} \mathbf{C}_x - \mathbf{X}$ $\tilde{\mathbf{X}} = \mathbf{X} + \mathbf{R}_x$ $\mathbf{Q}_{xx} = \frac{1}{\sigma_{x0}^2} \mathbf{N}^{-1}$ $\mathbf{Q}_{\tilde{x}\tilde{x}} = \frac{1}{\sigma_{x0}^2} \mathbf{A} \mathbf{N}^{-1} \mathbf{A}^T$ $e_x = \sqrt{\frac{\mathbf{R}_x^T \mathbf{R}_x}{r}}$	<p>X: Vector of observations $\tilde{\mathbf{X}}$: Vector of estimates A: Matrix of coefficients R: Vector of residuals C_x: Vector of unknowns (the coefficients in the polynomial adjustment) N: Cost or discrepancy matrix Q_{xx}: Observations cofactor matrix Q_{$\tilde{x}\tilde{x}$}: Estimates cofactor matrix e_x^2: Reference variance <i>r</i>: Number of degrees of freedom; $r = n - 3$, with n the number of observations</p>	(6)
---	---	-----

5

The above equations, solved for each individual stake, assume that all stakes are given equal weight. From these equations, \mathbf{C}_x is solved first to determine the coefficients of the second-degree polynomial adjustment. Then, the adjusted values $\mathbf{A} \mathbf{C}_x$ are calculated and the residuals \mathbf{R}_x computed, and finally the root-mean-square error in position e_x is calculated. The process is repeated for the corresponding equations for the Y coordinate, to get the vector of polynomial adjustment coefficients \mathbf{C}_y and the error estimate e_y .

10

We note that the above error estimates do not represent actual errors in the data points but an estimate of the average deviations (in a root-mean-square sense) of the data point positions with respect to their polynomial approximation. To evaluate the relative error in velocity, say, for the x component of the velocity, e_{v_x} , from the errors in position, e_x , and in timing, e_t , we use

15

$$\frac{e_{v_x}}{|v_x|} \cong \frac{e_x}{|\Delta x|} + \frac{e_t}{|\Delta t|} \quad (7)$$

Assuming that the error in timing is negligible as compared with the error in position, the above equation simplifies to

$$\frac{e_{v_x}}{|v_x|} \cong \frac{e_x}{|\Delta x|} \quad (8)$$

4. Description of the datasets

20

The shape file CNDA-ESP_SIMRAD_VELOCITY.shp available at PANGAEA database (<http://doi.pangaea.de/10.1594/PANGAEA.846791>) contains the position data for all stakes of Johnsons and Hurd glaciers for the period from 2000 to 2013. We describe below the contents of each individual field in the shape file.

25

- Field "t38_stake": The name of the stake under consideration (see stakes in Figure 2).
- Field "t38_t0": The zero time for the time variable. We set it as 01/01/1999 at 00:00 GMT.
- Field "t38_fecha": The date and time for the measurement, with "YYYYMMDDHHMMSS" format.
- Field "t38_inct": The period of time in days from "t38_t0" to "t38_fecha" (t_n in the above equations).
- Field "t38_x": X coordinate in meters (UTM 20S) for the stake (considered in an ideal vertical position, after correction for tilt, if applicable) (x_{t_n} in Equation 1).
- Field "t38_y": Y coordinate in meters (UTM 20S) for the stake (considered in an ideal vertical position, after correction for tilt, if applicable) (y_{t_n} in Equation 1).
- Field "t38_x_ide": X coordinate in meters (UTM 20S) for the position of the stake for the given time, calculated using the second-degree polynomial adjustment ($X_a(t_n)$ in Equation 3).
- Field "t38_y_ide": Y coordinate in meters (UTM 20S) for the position of the stake for the given time, calculated using the second-degree polynomial adjustment ($Y_a(t_n)$ in Equation 3).
- Field "t38_vx": X component for horizontal velocity of the stake for the given time, expressed in meters per year, calculated from the second-degree polynomial adjustment (v_x in Equation 5).

35



- Field “t38_vy”: Y component for horizontal velocity of the stake for the given time, expressed in meters per year, calculated from the second-degree polynomial adjustment (v_y in Equation 5).
- Field “t38_vxy”: Absolute value of horizontal velocity of the stake for the given time, expressed in meters per year, calculated from the X and Y components of the velocity obtained from the second-degree polynomial adjustment (v_{xy} in Equation 5).
- Field “t38_v_aci”: Azimuth for horizontal velocity of the stake, expressed in sexagesimal degrees, at the date of the measurement.
- Field “t38_err_x”: Root-mean-squared deviation for the X position of the stake, expressed in meters (e_x).
- Field “t38_err_y”: Root-mean-squared deviation for the Y position of the stake, expressed in meters (e_y).
- Field “t38_max_x”: Maximum error obtained for the X position of the stake, expressed in meters.
- Field “t38_max_y”: Maximum error obtained for the Y position of the stake, expressed in meters.
- Field “t38_ax”: The estimation for the “ a_x ” coefficient in the second-degree polynomial adjustment of the position X of the stake (a_x in Equation 3).
- Field “t38_bx”: The estimation for the “ b_x ” coefficient in the second-degree polynomial adjustment of the position X of the stake (b_x in Equation 3).
- Field “t38_cx”: The estimation for the “ c_x ” coefficient in the second-degree polynomial adjustment of the position X of the stake (c_x in Equation 3).
- Field “t38_ay”: The estimation for the “ a_y ” coefficient in the second-degree polynomial adjustment of the position Y of the stake (a_y in Equation 3).
- Field “t38_by”: The estimation for the “ b_y ” coefficient in the second-degree polynomial adjustment of the position Y of the stake (b_y in Equation 3).
- Field “t38_cy”: The estimation for the “ c_y ” coefficient in the second-degree polynomial adjustment of the position Y of the stake (c_y in Equation 3).

25 5. Results

The procedure described in the Methods section was applied to every stake, producing the polynomial coefficients and the estimated horizontal positioning misfits shown in Table 1. To give an idea of the order of magnitude of the velocities and their associated errors, and of their spatial variations, we have included in table A.1 in the Appendix the calculated velocities for a given time.

Stake	a_x	b_x	c_x	a_y	b_y	c_y	$e_{xy}(m)$
EH01	-0,0000000210	-0,0007499061	634706,536	-0,0000001022	-0,0006149926	3046974,077	±0,41
EH02	-0,0000000260	-0,0019490138	634314,937	0,0000000376	-0,0004418479	3046972,371	±0,31
EH03	0,0000000017	-0,0024338880	633957,992	0,0000000387	-0,0013300512	3046883,749	±0,25
EH04	0,0000000208	-0,0048559670	633602,733	0,0000000476	-0,0016952866	3046680,172	±0,24
EH05	0,0000000827	-0,0061748145	633322,971	0,0000000176	-0,0023909505	3046440,393	±0,15
EH06	0,0000001329	-0,0093454794	633066,469	0,0000001143	-0,0041399749	3046183,071	±0,30
EH07	0,0000002467	-0,0103102794	632769,911	0,0000001116	-0,0060335306	3045901,732	±0,32
EH08	0,0000002202	-0,0084839082	632511,087	0,0000002088	-0,0073298445	3045661,923	±0,31
EH10	-0,0000000115	-0,0021984650	634172,352	0,0000000196	0,0024960084	3047352,461	±0,18
EH11	-0,0000000060	-0,0033251769	633822,848	-0,0000000136	0,0040018668	3047646,355	±0,22
EH12	0,0000000058	-0,0029001077	633610,294	0,0000000058	0,0014133530	3047331,978	±0,50
EH13	0,0000000989	-0,0040996188	633908,319	0,0000000699	0,0034554549	3048276,555	±0,34
EH14	0,0000003949	-0,0066196722	633507,694	-0,0000000176	0,0011105547	3048060,055	±0,73
EH16	0,0000005378	-0,0121620919	633315,315	-0,0000003729	0,0088014677	3047778,378	±0,40
EH18	0,0000005266	-0,0079704077	632901,615	0,0000004036	0,0003691018	3047006,754	±0,45
EH19	0,0000001954	-0,0062025268	632821,167	0,0000000024	0,0013091532	3046916,708	±0,37
EH20	-0,0000000041	-0,0041607075	634641,903	0,0000000207	-0,0018151514	3046428,116	±0,36
EH21	0,0000000702	-0,0069464784	634311,036	-0,0000013781	-0,0125603214	3046415,468	±0,80
EH22	0,0000000418	-0,0019778722	633913,716	0,0000000351	-0,0024914249	3046250,139	±0,29



Stake	a_x	b_x	c_x	a_y	b_y	c_y	$e_{xy}(m)$
EH23	0,0000000850	-0,0074476651	633495,325	-0,0000000048	-0,0040643877	3046056,767	±0,29
EH25	0,0000001059	-0,0067918760	633252,533	0,0000000337	-0,0005615131	3046656,096	±0,19
EH26	0,0000000665	-0,0061374875	633283,461	0,0000000429	-0,0008986263	3046923,597	±0,27
EH27	0,0000001937	-0,0088012166	632945,263	0,0000000846	-0,0044487636	3045685,828	±0,31
EH28	0,0000003036	-0,0065784553	632626,203	0,0000002354	-0,0039697127	3046120,387	±0,35
EH30	-0,0000001863	-0,0031881664	634304,297	-0,0000004025	-0,0036269810	3046722,181	±1,28
EH31	0,0000004603	-0,0077532371	632191,166	0,0000002463	-0,0042862662	3045393,753	±0,49
EH32	0,0000004228	-0,0056874228	632981,252	0,0000000427	0,0003263696	3047088,876	±0,82
EH34	0,0000028295	-0,0221847247	633412,561	-0,0000004808	0,0070931604	3047929,344	±0,27
EH35	-0,0000001494	-0,0043610240	632899,866	0,0000001839	0,0002225731	3047005,252	±0,34
EH36	-0,0000000071	-0,0044714224	633378,639	-0,0000008964	0,0142598599	3047909,661	±1,35
EH37	0,0000001050	-0,0073407541	633291,187	-0,0000008597	0,0132842232	3047763,133	±0,83
EH38	0,0000000544	-0,0065644463	632376,878	-0,0000002724	-0,0024698302	3045462,670	±0,32
EH39	-0,0000000968	-0,0050881561	632296,779	-0,0000001033	-0,0031726807	3045423,513	±0,18
EH40	0,0000001909	-0,0080001652	633027,591	-0,0000000767	0,0064788163	3048074,317	±0,09
EH41	0,0000016791	-0,0191464499	632550,165	-0,0000027307	0,0262539089	3046960,654	±0,57
EJ03r	-0,0000001531	0,0100735338	634980,227	0,0000004252	0,0182063987	3047658,850	±0,76
EJ04	-0,0000003723	0,0061601161	635075,122	-0,0000005812	0,0259414549	3048020,871	±1,22
EJ05	0,0000000492	0,0011547502	635161,004	-0,0000003319	0,0333842531	3048375,872	±1,79
EJ05r	-0,0000004208	0,0031517495	635155,477	-0,0000019291	0,0363184602	3048344,319	±1,57
EJ06	-0,0000011073	-0,0042784868	635185,239	0,0000026943	0,0365926573	3048770,902	±3,07
EJ06r	0,0000016211	-0,0103198593	635192,433	-0,0000178994	0,0932484671	3048692,082	±3,82
EJ09	0,0000000101	-0,0000640752	636317,040	0,0000000306	-0,0003560897	3049669,857	±0,17
EJ10	-0,0000004307	-0,0068225266	636026,014	0,0000000111	-0,0054558209	3049450,521	±0,48
EJ11	-0,0000056619	-0,0199142185	635701,041	0,0000047076	-0,0040812151	3049278,770	±1,13
EJ14	-0,0000083181	0,0057260572	635350,340	0,0000190604	-0,0112107159	3048898,259	±4,77
EJ14r	0,0000026146	-0,0265096848	635395,318	-0,0000095539	0,0757322689	3048785,930	±1,54
EJ15	-0,0000115713	-0,0150161625	635587,960	0,0000177466	-0,0141862506	3049134,762	±4,52
EJ16	-0,0000012393	-0,0075342532	635564,261	0,0000014961	0,0227882933	3048586,798	±1,74
EJ16r	0,0000001769	-0,0118134174	635579,144	0,0000003110	0,0244004790	3048564,554	±1,49
EJ17	-0,0000073534	-0,0169745300	635820,867	0,0000070748	-0,0119983441	3049058,204	±1,84
EJ17r	-0,0000017878	-0,0295492517	635853,941	0,0000041007	-0,0069866948	3049052,604	±1,13
EJ18	-0,0000047503	-0,0128379987	635611,869	0,0000072099	0,0059753470	3048787,784	±3,62
EJ18r	-0,0000020714	-0,0198100707	635635,496	0,0000032380	0,0163894918	3048764,951	±2,08
EJ19r	-0,0000027156	-0,0347723467	635509,766	0,0000039813	0,0474550026	3048954,395	±2,89
EJ21	-0,0000000445	-0,0012778820	635920,791	0,0000000648	0,0020946021	3047848,965	±0,12
EJ22	0,0000000237	-0,0039724530	635745,947	0,0000000882	0,0088414448	3048083,628	±0,50
EJ23	-0,0000000349	-0,0046353861	635644,992	0,0000001090	0,0167557974	3048276,292	±0,87
EJ24	-0,0000000521	0,0032607734	635493,978	-0,0000001090	0,0152334223	3047502,873	±0,52
EJ26	-0,0000009008	-0,0103905425	636381,563	-0,0000001309	-0,0059871063	3049160,852	±0,70
EJ27	-0,0000014544	-0,0219763759	636156,950	0,0000004109	-0,0107406457	3049090,100	±1,48
EJ28	-0,0000031887	0,0011132529	636126,270	0,0000006713	0,0002700461	3048619,696	±1,33
EJ29	-0,0000001806	0,0115365135	634635,956	-0,0000000833	0,0097340264	3048288,181	±0,64
EJ30	0,0000002245	-0,0074398001	636727,973	0,0000000834	-0,0051238313	3049205,806	±0,13
EJ31	-0,0000002608	0,0064071706	635177,240	-0,0000004367	0,0119751394	3047018,091	±0,12



Stake	a_x	b_x	c_x	a_y	b_y	c_y	$e_{xy}(m)$
EJ32	-0.000002940	0.0083991531	634841.075	-0.000007905	0.0142317135	3047310.149	±0.27
EJ33	0.0000040527	-0.0808182396	636025.782	0.000004695	0.0104154497	3048835.009	±0.67
EJ34	-0.000001959	0.0026058368	634258.842	-0.000003753	0.0083361641	3047831.927	±0.09
EJ35	-0.0000030794	0.0145204365	636169.067	-0.0000019491	0.0189886987	3048680.544	±1.49
EJ36	0.0000098129	-0.1574078351	636082.069	-0.000007515	0.0481336713	3048977.865	±0.99
EJ37	-0.0000076218	0.0437382981	635654.292	0.0000010401	-0.0281496644	3049584.987	±2.83

Table 1. Adjusted functions, $X_a(t_n)$ and $Y_a(t_n)$, for all the stakes of the glaciers under study. It also shows the root-mean-squared deviation e_{xy} (in meters) made in the polynomial approximation of the position.

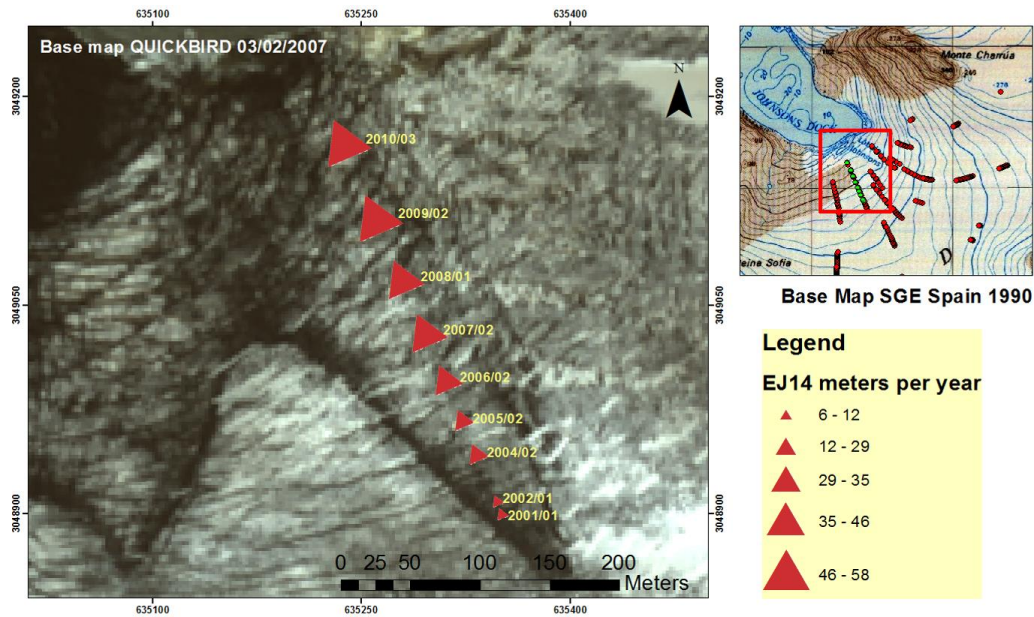


Figure 3. Map showing the time evolution of Stake EJ14. Horizontal velocities and times for various positions are shown. The stake was lost by calving during 2010-2011. The inset to the right shows the location of the image shown to the left (in the inset, EJ14 trajectory is shown in green). In this, and the following figures, UTM coordinates (sheet 20S) are indicated. The background image is a satellite photo of the QUICKBIRD system program (2007).

As an example, the detailed results for a particular stake, EJ14, are shown in Table 2 and Figure 3. The latter shows the position changes of the stake over time.

$$\begin{aligned}
 X_a(t_n) &= -0.0000083181 t_n^2 + 0.0057260572 t_n + 635350.340 \\
 Y_a(t_n) &= 0.0000190604 t_n^2 - 0.0112107159 t_n + 3048898.260 \\
 v_x &= -0.0000166362 t_n + 0.0057260572 \\
 v_y &= 0.0000381208 t_n - 0.0112107159 \\
 e_x &= \pm 1.69 \text{ m} \\
 e_y &= \pm 4.46 \text{ m} \\
 n &= 25 \\
 \text{Maximum velocity: } &57.31 \text{ m y}^{-1} \text{ on March 1, 2010.} \\
 \text{Maximum velocity azimuth: } &336.7019^\circ
 \end{aligned}$$

Table 2. Example of results for the adjustment by least squares of the position and the velocity of a stake (EJ14, near the calving front of Johnsons Glacier; see Figure 3), together with the root-mean squared deviations from the polynomial approximation for the position, as well as the maximum horizontal velocity and its direction.



5

In Figures 4 and 5 we show the horizontal velocities for all stakes of Hurd and Johnsons glaciers, respectively, for a given date (13/02/2013), calculated using the corresponding polynomial adjustments. Maximum velocities on Hurd Glacier are only of a few meters per day, and approach 10 m y^{-1} at the head of the unnamed glacier draining towards the south. Maximum velocities on Johnsons Glacier are much larger, up to several tens of meters per day, and reached near the calving front.

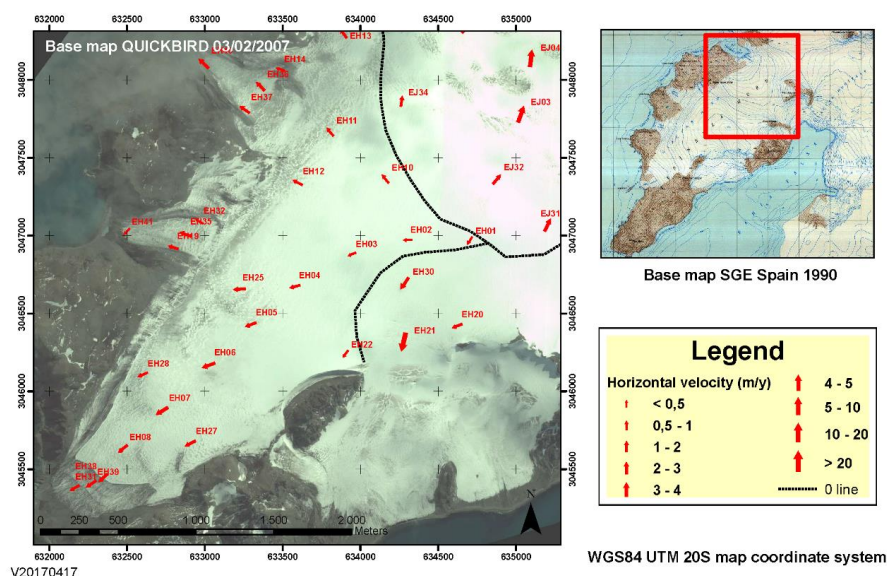


Figure 4. Horizontal velocity (modulus and direction) for Hurd Glacier stakes, estimated for 13/02/2013 using a second-degree polynomial adjustment. The dotted lines indicate the position of the ice divides.

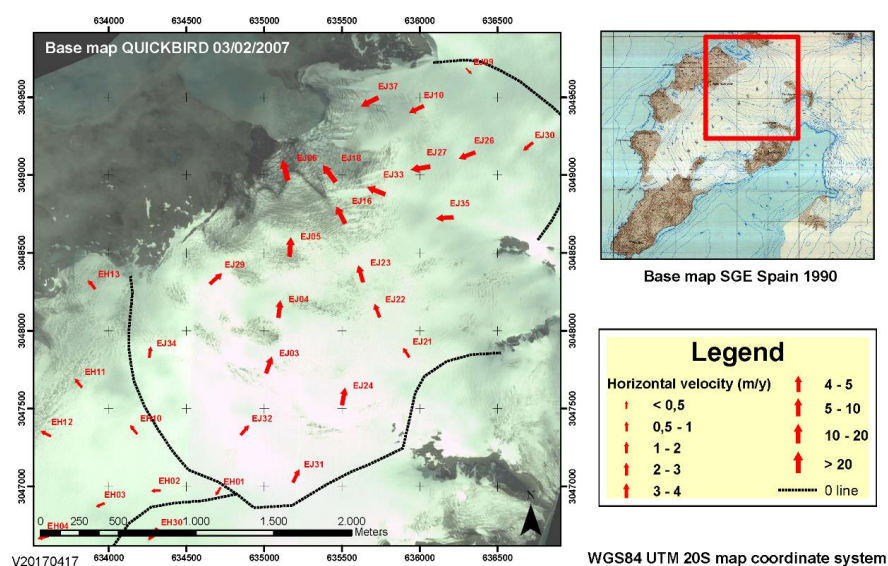
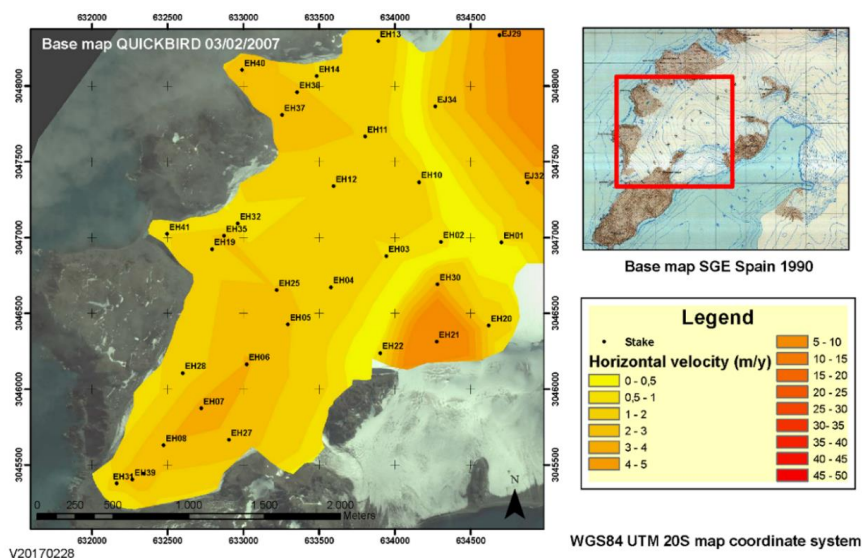


Figure 5. Horizontal velocity (modulus and direction) for Johnsons Glacier stakes estimated for 13/02/2013 using a second-degree polynomial adjustment. The dotted lines indicate the position of the ice divides.

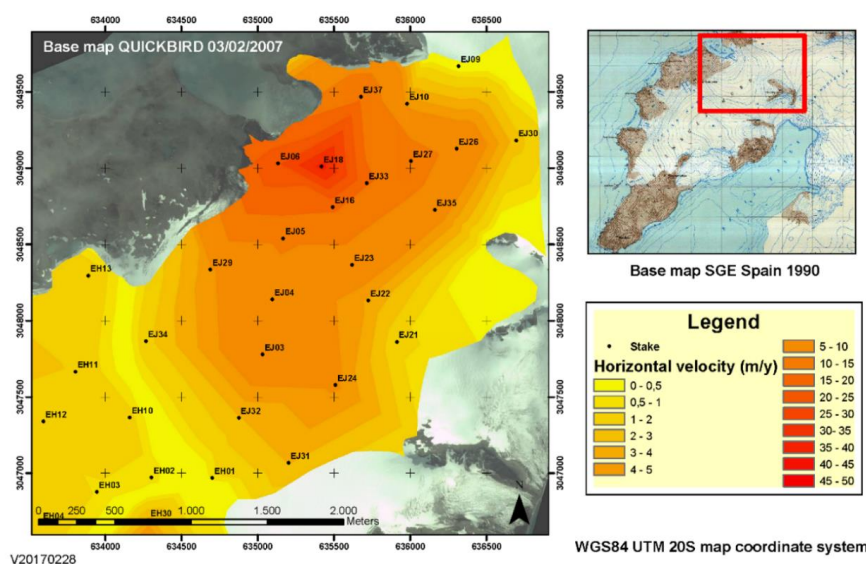


In Figures 6 and 7 we show the corresponding spatially-interpolated (nearest neighbour) contour lines for the absolute value of the velocities for the same date. In these latter figures, the zero velocity bands indicate the approximate location of the ice divides, where the component of horizontal velocity normal to the divide plane is zero by definition, and the component tangent to that plane is usually very small.



5

Figure 6. Absolute value of horizontal velocity for Hurd Glacier, estimated for 13/02/2013 using a second-degree polynomial adjustment. The yellow near-zero velocity band indicates the approximate location of the ice divides.



10

Figure 7. Absolute value of horizontal velocity for Johnsons Glacier, estimated for 13/02/2013 using a second-degree polynomial adjustment. The yellow near-zero velocity bands indicate the approximate location of the ice divides (except for the zone to the east, between UTM northing 3048000 and 3048500, which corresponds to thin frozen-to-bed ice on the upper part of a nunatak).



5. Discussion and summarizing conclusions

From the analysis of Figures 4-7, we see that Johnsons and Hurd glaciers show two markedly different dynamical regimes. Since Johnsons is a tidewater glacier, it shows a pattern of velocities increasing from the ice divides (where horizontal velocities are zero by definition) towards its calving front, where yearly-averaged velocities up to 65 m y^{-1} have been observed. On the contrary, Hurd is a land-terminating glacier, with much slower velocities (typically just a few m y^{-1}), in which the largest velocities are reached in its middle-to lower part (between stakes EH06-EH08; see Figure 6), where basal sliding is assumed to occur, and close to the land-terminating snouts the velocity field shows a decreasing pattern (this is particularly noticeable in the snouts of Sally Rocks and Las Palmas lobes; see Figure 6). Velocities are also high in the high-slope zones such as Argentina lobe and the upper part of Las Palmas lobe. Note that the high-velocity zone shown to the southeast of Hurd glacier, around stake EH21 (Fig. 6) does not really correspond to Hurd Glacier, but to an unnamed glacier flowing southwards, towards False Bay, which has extremely high slopes and is in fact a heavily crevassed icefall.

The decreasing velocities as we approach the land-terminating snouts have been attributed to the fact that the surficial cold ice layer reaches the bed in these zones, so the glacier is frozen to its bed and glacier movement is produced by internal deformation alone (no basal sliding). This is supported by both geomorphological observations, in particular the presence of compressional structures such as thrust faults close to the glacier termini (Molina et al., 2007; Molina, 2014) and to ground-penetrating radar studies that show that the cold ice layer reaches the bedrock in these zones (Navarro et al., 2009; Molina, 2014).

From the analysis of the polynomial interpolation of observed positions we see that a second-degree polynomial function (representing a uniformly accelerated motion) is sufficient to provide a fair adjustment to the observed position changes. The largest root-mean-square positioning error, of 5.54 m, is found for stake EJ18, which has an average horizontal velocity of ca. 30 m y^{-1} . Of course, one of the major drawbacks from the polynomial interpolation of the observed positions is that it does not allow to represent seasonal variations in glacier velocities, which are known to occur for the glaciers in this region (e.g. Osmanoğlu et al., 2014). In fact, we tried to add a sinusoidal function to the polynomial fit and the results were disappointing, although anticipated. This is because the positioning measurements are done only at the beginning and the end of each summer season, and thus do not allow to resolve yearly cycles. But the polynomial interpolation of all available positions for a given stake is just an example of what can be done with the available data. Calculations could be done for estimating e.g. summer-averaged velocities or winter-averaged velocities (for the “extended winter”, all of the year except for the summer season). Yet, this is still insufficient to study velocity variations at scales shorter than the seasonal. For this reason, perhaps the highest interest of the presented dataset is its use for tuning of free parameters of numerical models of glacier dynamics (e.g. Martín et al., 2003; Otero et al., 2010), since these models represent averaged velocities at time-step scales, which are often of the order of weeks (especially for steady-state models such as those cited, in which the time steps are applied to get the model reach a steady-state configuration). But even for transient models weekly time steps are usual (e.g. Otero et al., 2017). The available dataset is also useful for validation of remotely-sensed SAR velocities, with typical repeat cycles from a few days to several tens of days, up to 45 days for ALOS PALSAR.

Another shortcoming of the presented dataset is that it does not allow for an easy analysis of dynamical response to climate changes (such as those regionally observed by Oliva et al., 2016), because what is available is a Lagrangian velocity field (velocities measured at stakes that change their position with time), while what is needed for studying glacier velocity variations in response to climate changes is an Eulerian velocity field (velocities measured at fixed location in space).

From the above discussion, a desirable complement to the available in situ velocity dataset presented in this paper would be a continuous record of ice velocities at selected stakes.

Summarizing, the presented dataset is a useful source of input data for numerical models of glacier dynamics and for calibration-validation of remotely-sensed velocity data. It fills an observational data gap in the region peripheral to the Antarctic Peninsula, and it is thus expected that these data will contribute to the understanding of the dynamics of the ice masses in this region and their response to environmental changes.

Data availability

<http://doi.pangaea.de/10.1594/PANGAEA.846791>

Continuous velocity model for Johnsons and Hurd glaciers from 1999 to 2013, with link to model results in shapefile format.



Acknowledgements

This work was supported by grant CTM2014-56473-R from the Spanish National Plan of R&D.

References

- Bañón, M. and Vasallo, F. (2016). AEMET en la Antártida. Climatología y meteorología sinóptica en las estaciones meteorológicas españolas en la Antártida. 152 pp. AEMET, Madrid.
- Blindow, N., Suckro, S., Rückamp, M., Braun, M., Schindler, M., Breuer, B., Saurer, H., Simões, J.C. and Lange, M. (2010). Geometry and status of the King George Island ice cap (South Shetland Islands, Antarctica). *Annals of Glaciology*, 51, 103-109.
- Cuffey, K.M. and Paterson, W.S.B. (2010). *The Physics of Glaciers*, 4th Ed. Elsevier, Amsterdam.
- Ghilani, C.D. (2010). *Adjustment Computations. Spatial Data Analysis*. John Wiley & Sons, New Jersey.
- Hambrey, M. and Lawson, W. (2000): Structural styles and deformation fields in glaciers: a review. In: Maltman, A.J., Hubbard, B. and Hambrey, M.: *Deformation of Glacier Materials*. Glaciological Society, London, Special Publications, 176, 147-157.
- Hanson, B. 1995. A fully three-dimensional finite-element model applied to velocities on Storglaciären, Sweden. *Journal of Glaciology*, 41(137), 91-102.
- Joughin, I, Smith, B. and Abdalati, W. (2010). Glaciological advances made with interferometric synthetic aperture radar. *Journal of Glaciology*, 56(200), 1026-1042.
- Martín, C., Navarro, F.J., Otero, J., Cuadrado, M.L. and Corcuera, M.I. (2004). Three-dimensional modelling of the dynamics of Johnsons glacier (Livingston Island, Antarctica). *Annals of Glaciology*, 39, 1-8.
- Molina, C., Navarro, F., Calvet, J., García-Selles, D., and Lapazaran, J. (2007). Hurd Peninsula glaciers, Livingston Island, Antarctica, as indicators of regional warming: ice-volume changes during period 1956-2000, *Annals of Glaciology*, 46(1), 43-49.
- Navarro, F.J., Otero, J., Macheret, Y.Y., Vasilenko, E.V., Lapazaran, J.J., Ahlstrøm, A.P. and Machío, F. (2009). Radioglaciological studies on Hurd Peninsula glaciers, Livingston Island, Antarctica. *Annals of Glaciology*, 50 (51), 17-24.
- Navarro, F., Jonsell, U., Corcuera, M. and Martín-Español, A. (2013). Decelerated mass loss of Hurd and Johnsons glaciers, Livingston Island, Antarctic Peninsula. *Journal of Glaciology*, 59, 115-128.
- Osmanoğlu, B., Braun, M., Hock, R. and Navarro, F.J. (2013). Surface velocity and ice discharge of the ice cap on King George Island, Antarctica. *Annals of Glaciology*, 54(63), 111-119, doi: 10.3189/2013AoG63A517.
- Osmanoğlu, B., Navarro, F.J., Hock, R., Braun, M. and Corcuera, M.I. (2014). Surface velocity and mass balance of Livingston Island ice cap, Antarctica. *The Cryosphere*, 8, 1807-1823, doi: 10.5194/tc-8-1807-2014.
- Oliva, M., Navarro, F., Hrbáček, F., Hernández, A., Nývlt, D., Pereira, P., Ruiz-Fernández, J. and Trigo, R. (2016). Recent regional cooling of the Antarctic Peninsula and its impacts on the cryosphere. *Science of the Total Environment*, 580, 210-223, doi:10.1016/j.scitotenv.2016.12.030.
- Otero, J., Navarro, F.J., Lapazaran, J.J., Welty, E., Puczko, D. and Finkelnburg, R. (2017). Modeling the Controls on the Front Position of a Tidewater Glacier in Svalbard. *Frontiers in Earth Science*, 5, 29, doi:10.3389/feart.2017.00029.
- Otero, J., Navarro, F.J., Martín, C., Cuadrado, M.L. and Corcuera, M.I. (2010). A three-dimensional calving model: numerical experiments on Johnsons Glacier, Livingston Island, Antarctica. *Journal of Glaciology*, 56 (196), 200-214.
- Ren Jiaven, Qin Dahe, Petit, J.R., Jouzel, J., Wang Wenti, Liu Chen, Wang Shiaojun, Qian Songlin and Wang Xiaoxiang (1995). Glaciological studies in Nelson Island, Antarctica. *Journal of Glaciology*, 41(138), 408-412.
- Rignot, E. and Kanagaratnam, P. (2006). Changes in the velocity structure of the Greenland Ice Sheet. *Science*, 311(5763), 986-990.
- Rodríguez-Cielos, R., Aguirre de Mata, J., Díez-Galilea, A., Álvarez-Alonso, M., Rodríguez-Cielos, P. and Navarro, F.J. (2016). Geomatic methods applied to the study of the front position changes of Johnsons and Hurd Glaciers, Livingston Island, Antarctica, between 1957 and 2013. *Earth Syst. Sci. Data*, 8, 341-353, doi:10.5194/essd-8-341-2016.



- Rückamp, M., Blindow, N., Suckro, S., Braun, M. and Humbert, A. (2010). Dynamics of the ice cap on King George Island, Antarctica: field measurements and numerical simulations. *Annals of Glaciology*, 51, 80-90.
- Rückamp, M., Braun, M., Suckro, S. and Blindow, N. (2011). Observed glacial changes on the King George Island ice cap, Antarctica, in the last decade. *Global and Planetary Change*, 79, 99-109, doi:10.1016/j.gloplacha.2011.06.009.
- 5 Schellenberger, T., Dunse, T., Kääh, A., Kohler, J. and Reijmer, C.H. (2015). Surface speed and frontal ablation of Kronebreen and Kongsbreen, NW Svalbard, from SAR offset tracking. *The Cryosphere*, 9, 2339-2355, doi:10.5194/tc-9-2339-2015.
- SGE (1991). Isla Livingston: Península Hurd. Mapa topográfico 1:25 000. Servicio Geográfico del Ejército, Madrid.
- 10 Strozzi, T., Luckman, A., Murray, T., Wegmüller, U. and Werner, C. (2002). Glacier motion estimation using SAR offset-tracking procedures. *IEEE Transactions on Geoscience and Remote Sensing*, 40(11), 2384–2391.
- Strozzi, T., Kouraev, A., Wiesmann, A., Wegmüller, U., Sharov, A. and Werner, C. (2008). Estimation of Arctic glacier motion with satellite L-band SAR data. *Remote Sensing of the Environment*, 112(3), 636-645, doi:10.1016/j.rse.2007.06.007.
- 15 Wuite, J., Rott, H., Hetzenecker, M., Floricioiu, D., De Rydt, J., Gudmundsson, G.H., Nagler, T. and Kern, M. (2015). Evolution of surface velocities and ice discharge of Larsen B outlet glaciers from 1995 to 2013. *The Cryosphere*, 9, 957–969, doi:10.5194/tc-9-957-2015.
- Ximenis, L., Calvet, J., Enrique, J., Corbera, J., Fernández de Gamboa C. and Furdàda, G. (1999). The measurement of ice velocity, mass balance and thinning-rate on Johnsons Glacier, Livingston Island, South Shetland Islands, Antarctica, *Acta Geológica Hispánica*, 34, 403-409.
- 20 Ximenis, L., Calvet, J., García, D., Casas, J.M. and Sàbat, F. (2000). Folding in the Johnsons Glacier, Livingston Island, Antarctica. In: Maltman, A.J., Hubbard, B. and Hambrey, M.: *Deformation of Glacier Materials*. Glaciological Society, London, Special Publications, 176, 147-157.



Appendix A

Stake	X velocity (m y ⁻¹)	Y velocity (m y ⁻¹)	Horiz. velocity (m y ⁻¹)	Azimuth (°)	Error (m y ⁻¹)
EH01	-0,35	-0,61	0,70	210,09	±0,83
EH02	-0,81	-0,02	0,81	268,62	±0,90
EH03	-0,88	-0,34	0,95	248,93	±0,63
EH04	-1,69	-0,44	1,75	255,46	±0,60
EH05	-1,94	-0,81	2,10	247,45	±0,35
EH06	-2,91	-1,08	3,10	249,64	±0,57
EH07	-2,83	-1,78	3,35	237,85	±0,55
EH08	-2,27	-1,89	2,95	230,20	±0,38
EH10	-0,85	0,98	1,30	319,35	±0,39
EH11	-1,24	1,41	1,87	318,75	±0,69
EH12	-1,04	0,54	1,17	297,42	±1,31
EH13	-1,12	1,52	1,89	323,61	±0,89
EH14	-0,93	0,34	0,99	290,06	±1,34
EH19	-1,53	0,49	1,60	287,67	±1,12
EH20	-1,53	-0,58	1,64	249,14	±0,64
EH21	-2,27	-9,78	10,04	193,08	±0,71
EH22	-0,56	-0,78	0,96	215,99	±0,88
EH25	-2,08	-0,08	2,08	267,85	±0,61
EH27	-2,48	-1,31	2,81	242,27	±0,80
EH28	-1,26	-0,56	1,38	245,91	±0,73
EH30	-1,87	-2,84	3,40	213,30	±4,15
EH31	-1,10	-0,64	1,27	239,86	±0,96
EH32	-0,48	0,28	0,56	300,13	±2,76
EH35	-2,15	0,77	2,29	289,76	±1,02
EH36	-1,66	1,83	2,47	317,76	±2,10
EH37	-2,28	1,61	2,79	305,17	±1,30
EH38	-2,19	-1,93	2,92	228,65	±0,31
EH39	-2,22	-1,55	2,71	235,15	±0,27
EH40	-2,20	2,08	3,03	313,33	±0,09
EH41	-0,66	-0,71	0,97	223,07	±0,49
EJ03	2,42	6,57	7,00	20,25	±1,94
EJ04	0,85	7,28	7,33	6,64	±1,28
EJ05	0,61	10,94	10,95	3,17	±0,41
EJ06	-5,73	23,50	24,18	346,30	±1,72
EJ09	0,01	-0,01	0,02	135,41	±0,23
EJ10	-4,11	-1,95	4,55	244,64	±0,58
EJ16	-7,41	13,95	15,80	332,01	±1,48
EJ18	-22,56	29,31	36,99	322,42	±5,54
EJ21	-0,63	1,01	1,19	327,85	±0,13
EJ22	-1,36	3,56	3,81	339,08	±0,72
EJ23	-1,82	6,53	6,78	344,39	±0,56
EJ24	0,99	5,15	5,25	10,93	±0,56
EJ26	-7,18	-2,68	7,67	249,55	±0,87



EJ27	-13,50	-2,37	13,70	260,03	±2,80
EJ29	3,53	3,24	4,79	47,47	±1,24
EJ30	-1,87	-1,56	2,43	230,24	±0,15
EJ31	1,36	2,73	3,05	26,45	±0,11
EJ32	1,96	2,22	2,96	41,46	±0,65
EJ33	-14,23	5,57	15,28	291,38	±1,04
EJ34	0,21	1,63	1,64	7,45	±0,11
EJ35	-6,29	-0,41	6,31	266,30	±2,48

Table A.1. Horizontal velocities for Hurd and Johnsons Glacier stakes on 13/02/2013, calculated using the second-degree polynomial adjustment. From left to right: stake name, X and Y components of horizontal velocity, absolute value of horizontal velocity, azimuth of the horizontal velocity vector, and error estimate for the horizontal velocity. All velocities are expressed in meters per year.

5